

REPORT DOCUMENTATION PAGE

Form Approved
OMB NO. 0704-0188

Public Reporting burden for this collection of information is estimated to average 1 hour per response, including the time for reviewing instructions, searching existing data sources, gathering and maintaining the data needed, and completing and reviewing the collection of information. Send comment regarding this burden estimates or any other aspect of this collection of information, including suggestions for reducing this burden, to Washington Headquarters Services, Directorate for information Operations and Reports, 1215 Jefferson Davis Highway, Suite 1204, Arlington, VA 22202-4302, and to the Office of Management and Budget, Paperwork Reduction Project (0704-0188.) Washington, DC 20503.

1. AGENCY USE ONLY (Leave Blank)		2. REPORT DATE 12/6/99	3. REPORT TYPE AND DATES COVERED Final report, May 15, 1995 to May 14, 1999	
4. TITLE AND SUBTITLE Defect Engineering in Compound Semiconductor			5. FUNDING NUMBERS DAAH04-95-1-0322	
6. AUTHOR(S) Thomas F. Kuech				
7. PERFORMING ORGANIZATION NAME(S) AND ADDRESS(ES) University of Wisconsin, Department of Chemical Engineering 1415 Engineering Drive, Madison, WI, 53706			8. PERFORMING ORGANIZATION REPORT NUMBER FR144-EY60	
9. SPONSORING / MONITORING AGENCY NAME(S) AND ADDRESS(ES) U. S. Army Research Office P.O. Box 12211 Research Triangle Park, NC 27709-2211			10. SPONSORING / MONITORING AGENCY REPORT NUMBER ARO 3445037-MS	
11. SUPPLEMENTARY NOTES The views, opinions and/or findings contained in this report are those of the author(s) and should not be construed as an official Department of the Army position, policy or decision, unless so designated by other documentation.				
12 a. DISTRIBUTION / AVAILABILITY STATEMENT Approved for public release; distribution unlimited.			12 b. DISTRIBUTION CODE	
13. ABSTRACT (Maximum 200 words) The use of 'molecular' doping sources was extended to achieve new and controlled defect structures. The controlled introduction of oxygen from the oxygen doping source, $(C_2H_5)_2AlOC_2H_5$, developed under the previous proposal were used to track the oxygen-based defect levels across the $In_x(Al,Ga)_{1-x}P$, and $GaAs_yP_{1-y}$ band diagrams. These studies aided in assessment of the role of oxygen in the performance of devices made from these technologically important materials. The impact of the controlled development of the defect structure on the surface and interface morphology was determined. The work in this proposal utilized a strong combination of electrical and optical characterization techniques. Detailed measurements within the $(Al_yGa_{1-y})_{1-x}In_xP$ system has identified new defect structures exhibiting hysteretic effects impacting the performance in devices. A model suggesting that these defects are due to the interaction of point defects with the changing local environment around extended defects was developed. Additional work in conjunction with Wayne State University, was carried out concerning the incorporation and activity of Er in GaAs and GaN hosts.				
14. SUBJECT TERMS Defect Engineering, oxygen, Compound semiconductors			15. NUMBER OF PAGES 14	
			16. PRICE CODE	
17. SECURITY CLASSIFICATION OR REPORT UNCLASSIFIED	18. SECURITY CLASSIFICATION ON THIS PAGE UNCLASSIFIED	19. SECURITY CLASSIFICATION OF ABSTRACT UNCLASSIFIED	20. LIMITATION OF ABSTRACT UL	

NSN 7540-01-280-5500

Standard Form 298 (Rev.2-89)
Prescribed by ANSI Std. Z39-18
298-102

20000707 153

DETC QUALITY INSPECTED 4

REPORT DOCUMENTATION PAGE (SF298) (Continuation Sheet)

Statement of the Problem Studied

This project addressed the need for the development of controlled deep level structures in GaAs and InP-based materials, and was extended to rare-earth ions in GaN and GaAs. We extended the use of 'molecular' doping sources in order to achieve new and controlled defect structures. The controlled introduction of oxygen from the oxygen doping source, $(C_2H_5)_2AlOOC_2H_5$, developed under the previous proposal was used to track the oxygen-based defect levels across the $In_x(Al,Ga)_{1-x}P$, and $GaAs_yP_{1-y}$ band diagrams. These studies aid in assessing the role of oxygen in the performance of devices made from these technologically important materials. The co-introduction of unintentional oxygen was compared to the intentional incorporation through a series of collaborative efforts with industry. The impact of the controlled development of the defect structure on the surface and interface morphology was identified and assessed. This project utilized a strong combination of electrical and optical characterization techniques. In particular, we will apply near field optical spectroscopy to the study of individual defects in these materials. The scientific impact of this work is the further development of the 'defect engineering' of compound semiconductor materials and the elucidation of the role of these important defects. We have identified key defect structures in the $In_x(Al,Ga)_{1-x}P$ including new hysteretic defects previously unknown.

The following has representative studies from this work with more complete descriptions presented in the publications described at the end of this document.

1. Compensation of shallow impurities in oxygen-doped metalorganic vapor phase epitaxy grown GaAs

Introduction: Metalorganic vapor phase epitaxy (MOVPE) is widely used to grow high purity $Al_xGa_{1-x}As$ and high quality $Al_xGa_{1-x}As/GaAs$ interfaces, both of which are important in many opto-electronic and digital device structures. The growth of $Al_xGa_{1-x}As$, however, has always been difficult due to the reactive nature of both the Al-bearing alkyls and the $Al_xGa_{1-x}As$ growth surface. The initial studies of MOVPE $Al_xGa_{1-x}As$ have often reported materials that exhibited a low photoluminescence (PL) efficiency and a reduced free electron concentration, when co-doped with shallow donors. Both observations have been attributed to the incorporation of oxygen that results in deep level centers. These defects or defect complexes are effective non-radiative recombination centers, reducing the PL efficiency, and can compensate the shallow donors. The tendency of the oxygen deep centers to be electrically and optically active in both n- and p-type $Al_xGa_{1-x}As$ is not presently understood. This study presented a comparative study of the compensation of shallow acceptors and shallow donors in DEALO-doped GaAs grown by MOVPE. Specifically, C and Zn were used for p-type doping, and Si and Se for n-type doping. The compensation, if it occurs, should be mainly attributed to the Al-O based defects. Nevertheless, the possible interactions between oxygen and shallow dopants in the gas phase or near the growth front can not be excluded, a priori. While other dopant-oxygen complexes, such as the Zn-O complex in GaP, have been observed, we have studied a variety of shallow dopants in order to provide direct evidence of any possible oxygen-dopant interactions in our films.

Results: All samples were grown in a conventional horizontal low pressure (78 Torr) MOVPE reactor, using TMGa and arsine (AsH_3), on Si- or Zn-doped n^+ or p^+ (100) GaAs substrates with a 2° miscut in [010] direction toward (110) plane. Disilane (Si_2H_6), hydrogen selenide, dimethyl zinc, and carbon tetrachloride were employed for Si, Se, Zn, and C doping respectively. The controlled incorporation of the shallow dopants was established prior to the oxygen co-doping experiments. The preferred n-type species in GaAs is Si due to its low diffusion coefficient and low volatility. The linear relationship between $N_d - N_a$ in the GaAs and the Si_2H_6 mole fraction was observed in the EC-V profiles.

Si donors in GaAs are compensated by oxygen-related deep level centers. The compensation, $\Delta(N_d - N_a) = (N_d - N_a)_{no\ oxygen} - (N_d - N_a)_{oxygen}$, is a function of the DEALO mole fraction; $\Delta(N_d - N_a) \propto [DEALO]^2$. A power-law dependence, with the compensation being approximately 2. The incorporation of O and Al from DEALO is also not altered over the entire range of Si_2H_6 mole fractions. A similar compensation effect, as in the case of Si, was observed when Se was used as the shallow n-type dopant. The Se incorporation, at a concentration of $1.23 \times 10^{18} \text{ cm}^{-3}$, was not affected by the variation of DEALO concentrations. According to the EC-V results, a ~ second-order power-law dependence of the compensation on the DEALO mole fraction is also noted for this Se-doped sample. The amount of compensation is approximately equal to the total trap concentration, N_T , calculated from the DLTS peak heights. The measured defect structure is very similar regardless the use of Si or Se.

The DEALO-doping was found to lead to compensation in p-type GaAs for carbon and oxygen co-doped GaAs samples. A non-linear power-law dependence of the electrical compensation on the DEALO mole fraction is again noted, as in the case of n-type GaAs. The results from a second similar sample grown with a higher carbon concentration at $9.73 \times 10^{17} \text{ cm}^{-3}$. These samples possess a 2 slope behavior over the investigated range of DEALO gas phase mole fractions. The origin of this change in slope is not understood at present. The underlying deep level structure responsible for this p-type compensation was measured by DLTS. The DLTS spectra

exhibit a multiple-level structure, similar to the reported spectrum of $\text{Al}_{0.2}\text{Ga}_{0.8}\text{As}:\text{Zn}:\text{O}$. All the peak heights in the spectra of $\text{GaAs}:\text{C}:\text{O}$ samples increase with the DEALO mole fraction at a constant carbon concentration. Four separate deep level peaks in these spectra were identified and analyzed.

In this study, the DEALO-doped GaAs epitaxial layers, co-doped with a wide variety of shallow dopants, exhibited a comparable amount of dopant compensation in both n- and p-type cases, as a similar concentration of DEALO was applied during the growth. DLTS measurements on these materials have identified deep levels in both n- and p-type materials which are responsible for the observed compensation. In the case of n-type GaAs, the concentration of deep levels determined from DLTS quantitatively agreed with the observed trap-induced compensation levels. The measured total trap concentrations in p-type GaAs:O was found to be lower than the observed compensation by a factor of ~ 100 . It is not unlikely that the presence of additional levels in p-type GaAs:O with very large emission time constants, which are beyond our DLTS measurement capability, could account for part of the discrepancy. The chemical identity of shallow donors/acceptors does not appear to have a role in the amount of electrical compensation.

The striking similarity, in the compensation behavior and the multiple deep level structure, of oxygen deep centers in both p- and n-type GaAs suggests that these deep centers can have a variety of charge states, capturing both electrons and holes. The distribution of charge states over the defect population depends on the Fermi level position, which is in turn governed by the intentional shallow impurity doping and the oxygen concentration. While the specific microscopic nature of the oxygen-related deep centers is not presently understood, an analogy may be drawn from the electronic states associated with the lattice vacancy in silicon (V_{Si}). An isolated V_{Si} gives rise to four dangling bonds, each containing one electron which may occupy a lower energy configuration by forming new covalent bonds with the other neighboring atoms. The total defect energy may be lowered through a tetragonal Jahn-Teller distortion to overcome the electron-electron repulsion. V_{Si} can therefore assume a variety of charge states by gaining or losing electrons. The presence of five charge states of V_{Si} , ranging from a double donor to a double acceptor, have been experimentally observed. In bulk-grown GaAs, the electrically active oxygen defect is assumed to be an off-centered, substitutional oxygen on an arsenic vacancy ($V_{\text{As}}\text{-O}$ complex) consisting of a 'Ga₂O molecule' and a Ga-Ga bridging bond. In DEALO-doped GaAs, the Ga₂O molecule could be replaced by an $\text{Al}_x\text{Ga}_{2-x}\text{O}$ species since the Al-O bonding is the main driving force for oxygen incorporation, with Ga-Ga, Al-Ga, or Al-Al back bridging bonds. We have previously attributed the observed multiple deep level structure in DEALO-doped GaAs to the variation in the number of Al nearest-neighbors to oxygen. This identification is supported by the growth and incorporation behavior of oxygen from DEALO into GaAs. The dangling bonds on the two constituents of the back bridging bond could be quite reactive, forming states quite similar in origin to the V_{Si} . As in the case of the V_{Si} , the Fermi level position determine the charge distribution with these defect states.

Conclusion: The intentional oxygen incorporation, using DEALO, in MOVPE GaAs was found to compensate C and Zn shallow acceptors as well as Si and Se shallow donors, due to the oxygen-related multiple deep levels within the GaAs bandgap. DLTS was used to characterize these oxygen deep centers. No changes in compensation or the DLTS characteristics were detected by varying the chemical identities of the shallow dopants, and the possible interactions between these shallow impurities and oxygen are not present. In particular, the recently inferred complex of Se and O in $\text{Al}_x\text{Ga}_{1-x}\text{As}$, leading to the lack of observed effects typically attributed to oxygen in these Se-doped materials, was not observed in our study. The total measured trap concentration from DLTS can account for

the observed compensation only in n-type GaAs:O. The total trap concentration in p-type GaAs:O was found to be lower than the observed compensation by a factor of ~ 100 . These oxygen deep centers appear to be able to possess at least two net charge states, positive (donors) or negative (acceptors) in nature, that are both energetically favorable. These multiple charge states could have contributed, in part, to the multiple deep level structure of GaAs:O.

2. Intrinsic and Oxygen-related Deep Level Defects in $\text{In}_{0.5}(\text{Al}_x\text{Ga}_{1-x})_{0.5}\text{P}$ Grown by Metal-Organic Vapor Phase Epitaxy

Introduction: Oxygen-related defects in Al-containing semiconductors can degrade luminescence efficiency and reduce free carrier lifetime affecting the performance of light emitting devices. We have used the oxygen-doping source, diethylaluminum ethoxide, $(\text{C}_2\text{H}_5)_2\text{AlOC}_2\text{H}_5$, to intentionally incorporate oxygen-related defects during growth of $\text{In}_{0.5}(\text{Al}_x\text{Ga}_{1-x})_{0.5}\text{P}$ by Metal-Organic Vapor Phase Epitaxy (MOVPE). Our investigations have identified several defects which are present in non-intentionally oxygen-doped n-type $\text{In}_{0.5}(\text{Al}_x\text{Ga}_{1-x})_{0.5}\text{P}$ as well as those due to oxygen. Oxygen introduces defect states near the middle of the band gap. Deep level transient spectroscopy and photoluminescence data obtained over the range of composition $0 < x < 1$, delineating the trends in defect structure with alloy composition.

Results: Several defect-derived energy levels are present in the DLTS spectra of nominally oxygen-free $\text{In}_{0.5}(\text{Al}_x\text{Ga}_{1-x})_{0.5}\text{P}$ offset from each

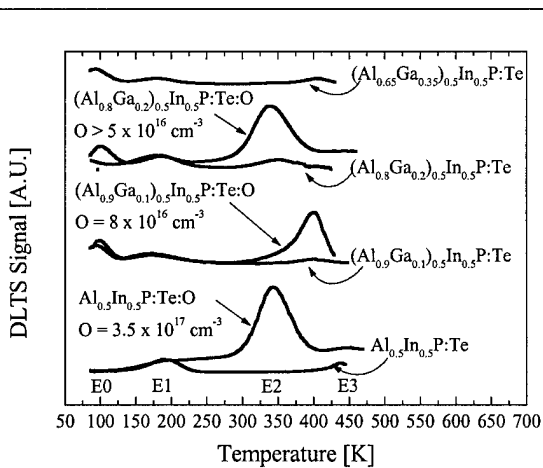


Figure 2.1. DLTS spectra for $\text{In}_{0.5}(\text{Al}_x\text{Ga}_{1-x})_{0.5}\text{P}$ with and without intentionally incorporated oxygen. The presence of several 'intrinsic' defects at low and high measurement temperatures are also observed. DLTS measurement conditions were -2 V reverse bias with a 1.5 V, 1 msec filling pulse, and a 50 ms period. The rate window utilized for the data shown above is 21.5 msec.

other for direct comparison. Figure 2.1 presents several DLTS spectra for $\text{In}_{0.5}(\text{Al}_x\text{Ga}_{1-x})_{0.5}\text{P}$ with $x = 1, 0.9, 0.8,$ and 0.65 . DLTS measurements for the oxygen-doped material and the nominally oxygen-free control samples are compared in Figure 2.1. For the case of the ternary alloy, $\text{Al}_{0.5}\text{In}_{0.5}\text{P}$, several levels are superimposed, with only the defect peak E2 being clearly present. For $\text{In}_{0.5}(\text{Al}_{0.8}\text{Ga}_{0.2})_{0.5}\text{P}$, two peaks are present below room temperature; the previously observed E1 level at 170 K and another at 90 K designated E0. Defect E0 has also been observed previously in Se-doped $\text{In}_{0.5}(\text{Al}_x\text{Ga}_{1-x})_{0.5}\text{P}$ and has been proposed to be a DX-related state. This assignment seems more plausible since we were not able to saturate this level with the pulse widths available with our DLTS system. The oxygen-related defect appears at a similar temperature as for $\text{Al}_{0.5}\text{In}_{0.5}\text{P}$. $\text{In}_{0.5}(\text{Al}_{0.9}\text{Ga}_{0.1})_{0.5}\text{P}$ was also investigated, but the oxygen concentration in this sample was significantly less than the other samples shown in Figure 2.1. This reduced oxygen concentration is apparent as the magnitude of the E2 defect peak is less than in the other alloy compositions and is superimposed with the E3 defect peak. The DLTS peak was deconvolved into two separate features and a data regression was used to obtain the peak positions. The E2 peak was identified in the samples with different alloy compositions after such data analysis.

The trend in the defect activation energies as a function of Al composition for the defects found in $\text{In}_{0.5}(\text{Al}_x\text{Ga}_{1-x})_{0.5}\text{P}$ is shown in Figure 2.2 along with the major band structure features. The oxygen-related defects, E2, appear to be relatively independent of the alloy composition over the range studied, lying ~ 0.9 eV below the conduction band. This is consistent with the previous work that assigned the oxygen-related defect to an energy level between 0.9 and 1.1 eV below the conduction band edge. This conclusion allows speculation on the origins of the 0.9 eV level identified in $\text{In}_x\text{Ga}_{1-x}\text{P}$. This level could be due to residual oxygen contamination. The shallower, 'intrinsic' defects appear to follow the X conduction band edge. The E0 defect concentration in these alloys depends on the Al-to-Ga ratio. For $\text{Al}_{0.5}\text{In}_{0.5}\text{P}$, there was no detectable concentration of the defect associated with the E0 spectral feature with only the E1 related peak being observed in the DLTS measurements. As the Ga mole fraction in the alloy is increased, forming the quaternary alloy, the E0 peak could be observed in the measured DLTS spectra with the concentration of this defect increasing from $7.5 \times 10^{15} \text{ cm}^{-3}$ for $\text{In}_{0.5}(\text{Al}_{0.9}\text{Ga}_{0.1})_{0.5}\text{P}$ to $2.3 \times 10^{16} \text{ cm}^{-3}$ for $\text{In}_{0.5}(\text{Al}_{0.8}\text{Ga}_{0.2})_{0.5}\text{P}$. The concentration of E1 varied by only 30 percent from $\text{Al}_{0.5}\text{In}_{0.5}\text{P}$ to $\text{In}_{0.5}(\text{Al}_{0.8}\text{Ga}_{0.2})_{0.5}\text{P}$.

Conclusions: Defects related to the incorporation of oxygen into $\text{In}_{0.5}(\text{Al}_x\text{Ga}_{1-x})_{0.5}\text{P}$ have been identified. The emission energy of these oxygen-related defects is ~ 0.9 eV below the conduction band edge, near the midgap for this alloy system. Several 'intrinsic' defects were also determined over the alloy system and appear in both the nominally non-oxygen-doped as well as intentionally oxygen-doped films. Defect E1 is suggested to be due to a stoichiometric defect, possibly a phosphorus vacancy. Defect E0, which becomes more prominent with increasing Ga content, is believed to be the DX center in this material system. A fourth defect, E3, appears at high measurement temperatures and exhibits an emission behavior that is dependent on both thermal history and biasing of the sample. The intentional oxygen doping of these materials has allowed identification of the specific defect due to oxygen incorporation.

3. Oxygen-Related Defects in Low Phosphorous Content $\text{GaAs}_{1-y}\text{P}_y$ Grown by MOVPE

Introduction: $\text{GaAs}_{1-y}\text{P}_y$ alloys have been used extensively for light emitting devices (LEDs) in the red and orange spectral regions. Due to this wide use, several investigations of the electrical and optical characteristics of $\text{GaAs}_{1-y}\text{P}_y$ have been performed on materials grown by a variety of techniques. One impurity common to all growth techniques is oxygen. Oxygen-induced deep levels in binary compound semiconductors, especially GaAs and GaP, have been previously studied in depth. In GaP, electrically active oxygen is known to occupy a site of tetrahedral symmetry, substituting for phosphorus. The lattice location of oxygen in GaAs is less well defined. Studies on GaAs, grown by the Liquid Encapsulated Czochralski (LEC) or Horizontal Bridgman (HB) techniques, assign an off-center substitutional site, O_{As} , to electrically active oxygen. Electrically inactive oxygen resides in an interstitial site. The effect of

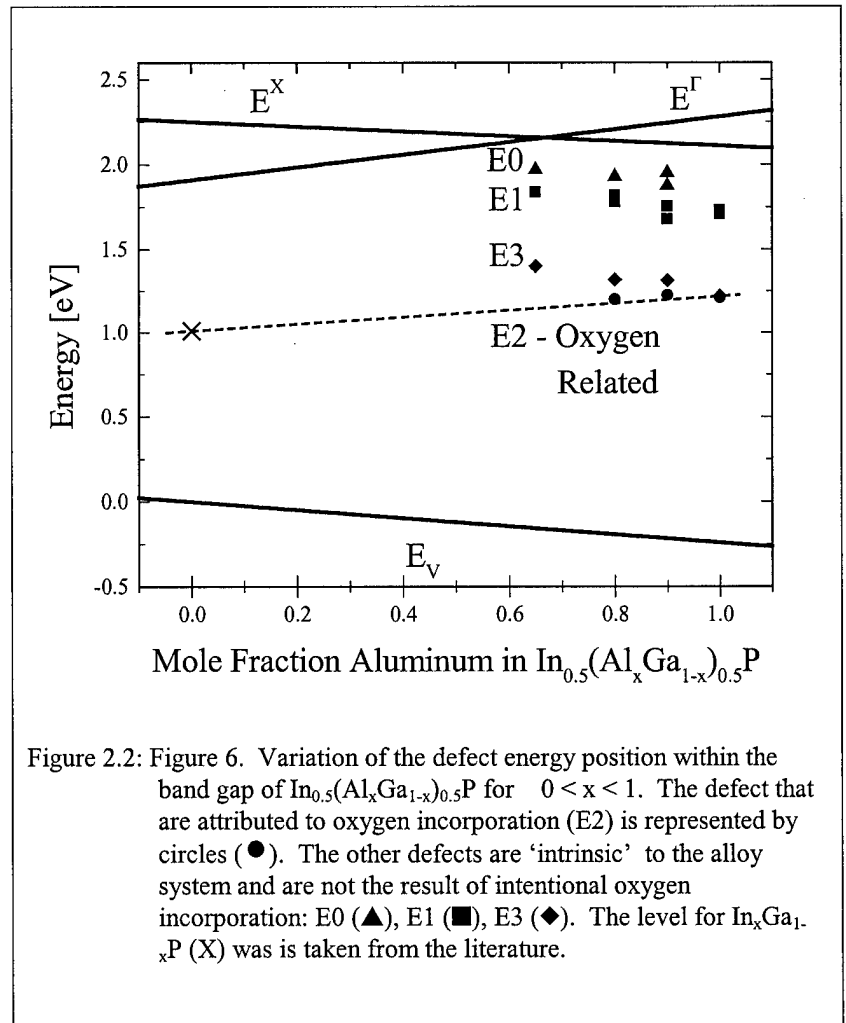


Figure 2.2: Figure 6. Variation of the defect energy position within the band gap of $\text{In}_{0.5}(\text{Al}_x\text{Ga}_{1-x})_{0.5}\text{P}$ for $0 < x < 1$. The defect that are attributed to oxygen incorporation (E2) is represented by circles (●). The other defects are 'intrinsic' to the alloy system and are not the result of intentional oxygen incorporation: E0 (▲), E1 (■), E3 (◆). The level for $\text{In}_x\text{Ga}_{1-x}\text{P}$ (X) was taken from the literature.

oxygen on $\text{GaAs}_{1-y}\text{P}_y$ has not been as thoroughly studied as in its component binaries. Changing the composition of the alloy provides a means by which the effect of the microscopic environment on the defect characteristics can be determined. Some investigations have been performed on the energy position of the oxygen level over the range of $\text{GaAs}_{0.35}\text{P}_{0.65}$ to GaP using photoluminescence spectroscopy. Extrapolation of this data, obtained for high phosphorous content $\text{GaAs}_{1-y}\text{P}_y$, has assigned a level of $E_c - E_t = 0.79$ eV for the O_{As} defect in GaAs. The work reported here presents results of Deep Level Transient Spectroscopy (DLTS) and growth studies of oxygen-related defects in low phosphorous content $\text{GaAs}_{1-y}\text{P}_y$ ($x < 0.17$). When combined with existing data, a complete picture of the nature of the oxygen defect in $\text{GaAs}_{1-y}\text{P}_y$ alloys over the entire composition range is obtained.

Results: Samples of $\text{GaAs}_{1-y}\text{P}_y$ were grown in a horizontal, low pressure (78 Torr) reactor in a hydrogen carrier gas at 600°C with a $V/\text{III} \sim 100$. Trimethyl gallium (TMGa), arsine (AsH_3), and phosphine (PH_3) were used as growth precursors. Disilane, diluted to 10 ppm in hydrogen, was used for n-type doping. Oxygen was incorporated using the molecular dopant source diethylaluminum ethoxide (DEAlO).

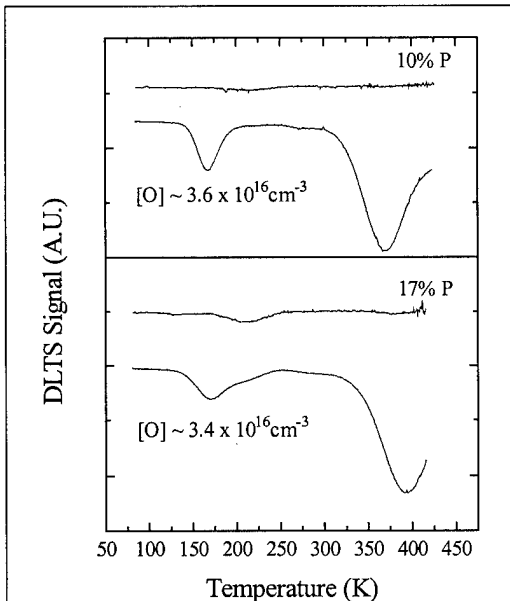


Figure 3.1. A characteristic DLTS spectra for the samples studied. Samples were measured at a reverse bias of -1 Volt, pulsing to 0 Volt for 1 ms. The period used was 500 ms with a rate window of 21.5 ms.

As the composition of phosphorus in the alloy is increased, the major oxygen-related DLTS peaks are shifted toward higher temperatures. Determination of the higher energy peaks required either a longer rate window or higher measurement temperatures. Such experimental conditions were not accessible in this study, due to limitations in the DLTS system and the degradation of the Schottky diode at high temperatures. It should be noted that the total number of defects measured by DLTS is approximately one order of magnitude less than the total amount of compensation measured by ECV. Also, the effect of incomplete trap filling has been accounted for in our data analysis. This difference between DLTS-measured trap concentration and total compensation indicates the presence of at least one other defect at a significant concentration deeper in the energy gap. The oxygen-induced energy levels determined by DLTS are plotted as a function of composition in Figure 3.2. The energy position deduced from PL peak position for phosphorous-rich $\text{GaAs}_{1-y}\text{P}_y$ ($y > 0.65$) implanted with oxygen is plotted along with a proposed linear extrapolation to the position of the oxygen-related defect in GaAs. The principal levels determined in this study agree quite well with this simple linear extrapolation from the previously reported values. Deviation from this linear extrapolation may be attributed to the variation in the energy level position of oxygen due to the co-incorporation of Al. Previous studies on deep levels have proposed different theories concerning the relationship of the specific band structure features to the defect deep level energy and electronic structure. It has been proposed that localized defects, like oxygen, are linked to the bulk of the electronic states. In Figure 2.2, the centroid of the conduction band density of states is plotted, assuming a linear interpolation with composition. Defect E2 appears to track the bulk of the electronic states, not the vacuum level or a

particular bandedge as proposed for some deep impurities.

Conclusions: This study has investigated the incorporation of oxygen-related defects into $\text{GaAs}_{1-y}\text{P}_y$ using the oxygen-containing precursor, DEAlO. The study indicates that the amount of oxygen incorporated into the alloy is reduced compared to GaAs for the same gas phase DEAlO mole fraction. DLTS has been used to measure the position of the oxygen related defects in approximately the upper half of the bandgap. Comparison of the results with data taken for the high phosphorous content $\text{GaAs}_{1-y}\text{P}_y$ indicate that the oxygen-related defect may follow the bulk of the conduction band states and not a vacuum reference level. PL measurements show that the incorporation of oxygen reduces band-to-band luminescence and introduces new features in the infrared region.

4. High-temperature hysteresis effects in $(\text{Al}_x\text{Ga}_{1-x})_{0.5}\text{In}_{0.5}\text{P}$ ($x > 0.65$)

Introduction: $(\text{Al}_x\text{Ga}_{1-x})_{0.5}\text{In}_{0.5}\text{P}$ is a wide bandgap, quaternary semiconductor, which can be lattice matched to GaAs. For these reasons $(\text{Al}_x\text{Ga}_{1-x})_{0.5}\text{In}_{0.5}\text{P}$ is widely used in optoelectronic devices, especially visible light emitters. Several studies of the defects present in this material system have been performed on samples grown by a variety of methods. Several defects states are present in the upper half of the bandgap. Two defects with

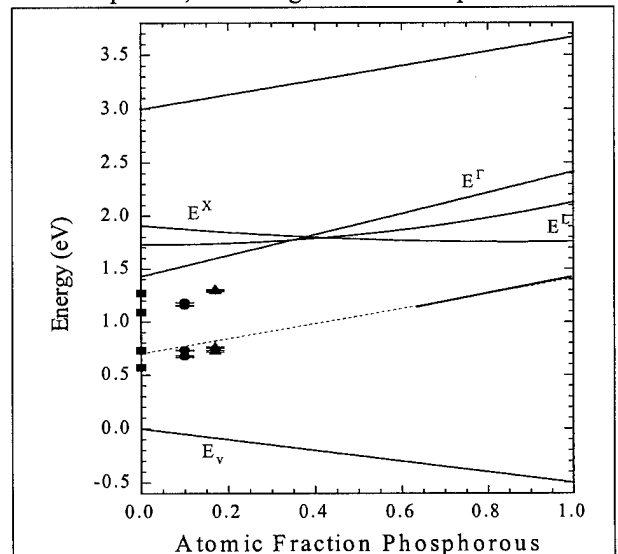


Figure 3.2: The oxygen related defect energy levels are presented as a function of the alloy composition assuming the GaAs valence band as the energy reference. The valence band discontinuity between GaAs and GaP is assumed to be linear. Major features of band structure are plotted for reference. The solid curve at high P-contents and for GaAs:O represent data from the previous work.

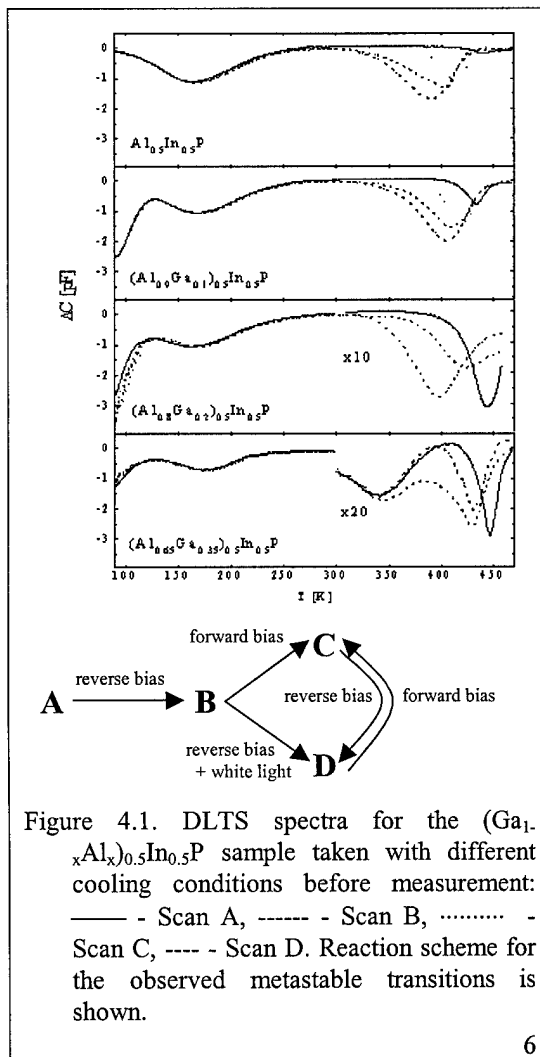
energies of approximately 0.2 and 0.4 eV have been assigned as DX-type centers. Defects further in the bandgap have been correlated to the presence of oxygen. These studies have focused on the effect of unintentional oxygen incorporation on the deep level structure, making direct identification of these features as being due to oxygen-related defects or intrinsic defects difficult. These studies utilized deep level transient spectroscopy and its variations, but were limited by the maximum temperature at which they were able to observe thermal emission. We have investigated $(\text{Al}_x\text{Ga}_{1-x})_{0.5}\text{In}_{0.5}\text{P}$ ($0.65 < x < 1.0$) doped with Te, and observe several electron traps in the upper half of the bandgap. Defect states emitting above 390 K exhibit hysteretic behaviour in the observed DLTS spectrum. Metastable states exhibiting a similar effect were observed in undoped and Fe-doped InP. Metastable states are also been associated with interstitial iron-substitutional acceptor pairs in silicon. Carbon-related defects, exhibiting metastable behavior, have been observed in silicon following irradiation with electrons. In these cases it was determined that the metastability was due to different charge states of the defect complex that could be controlled by biasing the sampling under test or a defect reaction that could be controlled by a combination of applied bias and temperature. Hysteresis effects have not been previously observed in $(\text{Al}_x\text{Ga}_{1-x})_{0.5}\text{In}_{0.5}\text{P}$ or for such an energetically deep level.

Results: Samples were grown by metal-organic vapor phase epitaxy (MOVPE) at 800°C at a pressure of 80 Torr using trimethylindium, trimethylgallium and trimethylaluminum as cation sources. Pure PH_3 and AsH_3 were used as anion precursors. Samples consisted of a nominally 1 μm layer of $(\text{Al}_x\text{Ga}_{1-x})_{0.5}\text{In}_{0.5}\text{P}$ alloy grown on a GaAs substrate. All the samples were uniformly doped with a donor concentration of nominally $3 \times 10^{17}\text{cm}^{-3}$, using diethyltelluride. Secondary Ion Mass Spectrometry (SIMS) on similar samples indicated the oxygen, silicon and carbon concentrations were below the detection limit of $1 \times 10^{16}\text{cm}^{-3}$.

The hysteresis effects observed in the DLTS spectra depended on the amount of thermal and electrical stress applied during or between measurements. DLTS spectra for $(\text{Al}_x\text{Ga}_{1-x})_{0.5}\text{In}_{0.5}\text{P}$ ($x = 1.0, 0.9, 0.8,$ and 0.65), obtained during four successive measurements, are presented in Figure 4.1. Scan A, the first spectrum measured for each sample, was the first time the diode had been exposed to high temperatures and high electric fields in combination. The second scan, Scan B, was performed immediately after Scan A had finished and utilized the same measurement parameters. During cooling, the sample was exposed to 2 V reverse bias. After Scan B, the diode was stressed by maintaining a forward bias current of approximately 6 mA/cm^2 during cooling from 470 K. At 300 K the diode was reconnected to the DLTS equipment, and the sample was cooled to 80 K under reverse bias. Scan C was then taken utilizing the same measurement conditions as for Scans A and B. After Scan C, the sample was cooled under 2 V reverse bias and a fourth scan, Scan D, was taken using the standard measurement conditions.

Over the temperature range of 82 to 280 K, the DLTS spectra of all samples are independent of the thermal and electrical conditions imposed on the diode. Within this temperature region two electron traps were observed, represented by DLTS peaks at 90 K and 170 K, labeled E0 and E1, respectively. The position of these levels does not vary significantly with the addition of gallium to the alloy. Above 390 K, a single peak was observed in all samples. The position and amplitude of this feature is strongly dependent on the history of the sample. In $\text{Al}_{0.5}\text{In}_{0.5}\text{P}$, Scan A reveals a small, broad peak at 440 K (state A). During Scan B, this high temperature peak shifted to 400 K and increased in amplitude to approximately six times the amplitude measured in Scan A (state B). Scan C produced a much narrower peak shifted to 415 K (state C). Scan D resulted in the feature being shifted to 395 K and becoming much broader (state D). For $(\text{Al}_{0.9}\text{Ga}_{0.1})_{0.5}\text{In}_{0.5}\text{P}$ at temperatures above 390 K, one peak was also observed. The position of this peak changes in a similar manner as described for $\text{Al}_{0.5}\text{In}_{0.5}\text{P}$. The changes in peak amplitude follow the trends observed for $\text{Al}_{0.5}\text{In}_{0.5}\text{P}$, with the total amplitude of the peak increasing from Scan A to Scan B, however, the effect is not as strong as observed in $\text{Al}_{0.5}\text{In}_{0.5}\text{P}$. As the amount of Ga in the alloy is increased to $(\text{Al}_{0.8}\text{Ga}_{0.2})_{0.5}\text{In}_{0.5}\text{P}$ and $(\text{Al}_{0.65}\text{Ga}_{0.35})_{0.5}\text{In}_{0.5}\text{P}$, the amplitude of the signal decreases substantially. Shifts in peak position are observed as the sample is cycled through the temperature and electrical conditions (Scans A through D), but these shifts are not as large as for $\text{Al}_{0.5}\text{In}_{0.5}\text{P}$ and $(\text{Al}_{0.9}\text{Ga}_{0.1})_{0.5}\text{In}_{0.5}\text{P}$. The amplitude of the peaks has an opposite trend, showing a decrease from Scan A to Scan B. A small peak at 345 K in the $(\text{Al}_{0.65}\text{Ga}_{0.35})_{0.5}\text{In}_{0.5}\text{P}$ is due to the presence of oxygen in this film.

It is noted that thermal and electrical stressing of the material can lead to complex behaviors of the observed defects. The simplest interpretation of these DLTS results would be the presence of an electron trap with several metastable states deep in the bandgap. Changes introduced by different biasing conditions at high temperature were stable over long periods of time after cooling the sample to room temperature. The application of various electrical stresses, at room temperature, did not affect the behavior of the DLTS spectra during measurement. These observations and the fact that it is possible to observe electron capture and emission from different states during successive DLTS measurements suggests transformations between states are connected with an electronic change in the defect configuration, which may remain stable at room temperature over extended



periods of time. Although these changes are similar to those observed for the DX center in $\text{Al}_x\text{Ga}_{1-x}\text{As}$ or $\text{GaAs}_{1-y}\text{P}_y$ or defects in InP, the electronic structure of these defects is more complex. In our $(\text{Al}_x\text{Ga}_{1-x})_{0.5}\text{In}_{0.5}\text{P}$ samples, we observed four metastable states, with different relations between peak amplitude depending on the Ga composition. The multiplicity of states associated within these DLTS spectra suggests a complex defect arrangement. Our results would suggest that a simple rearrangement associated with the local atomic rearrangement of a donor-intrinsic defect complex, which has been suggested as a model for DX, may be insufficient to explain the present results. Other workers have suggested that a more complex defect electronic spectrum could result from the interaction of a carrier with an extended defect of unknown origin. In such a defect structure, the local electric field of the charged or discharged extended defect may significantly change capture barrier and the observed emission energy, resulting in changes in the DLTS peak position, amplitude, and breadth. Injecting current while at high temperatures may cause the defect to charge and affect the capture barrier. The nature of such a charged, extended defect is unknown. The simplest defect, a misfit related dislocation, may be unlikely due to the pseudomorphic nature of our films. Defects could be introduced during cooling due the difference in the coefficient of thermal expansion between the GaAs substrate and the alloy film. Additional work is needed to identify the atomic origins of these states and their relationship to the growth and utility of these materials.

Conclusions: We have studied $(\text{Al}_x\text{Ga}_{1-x})_{0.5}\text{In}_{0.5}\text{P}$ doped with tellurium using Deep Level Transient Spectroscopy and associated electrical measurements. Several defect states are observed in the upper half of the band gap, that are believed to be intrinsic to the alloy system as well as related to the tellurium donors. Defects observed at measurement temperatures above 390 K exhibit a hysteretic behavior. The observed spectra depend on the biasing conditions applied to the Schottky diode during cooling. The hysteretic behavior suggests the existence of different defect configurations, which can be accessed at high measurement temperatures, but remain stable below 300 K.

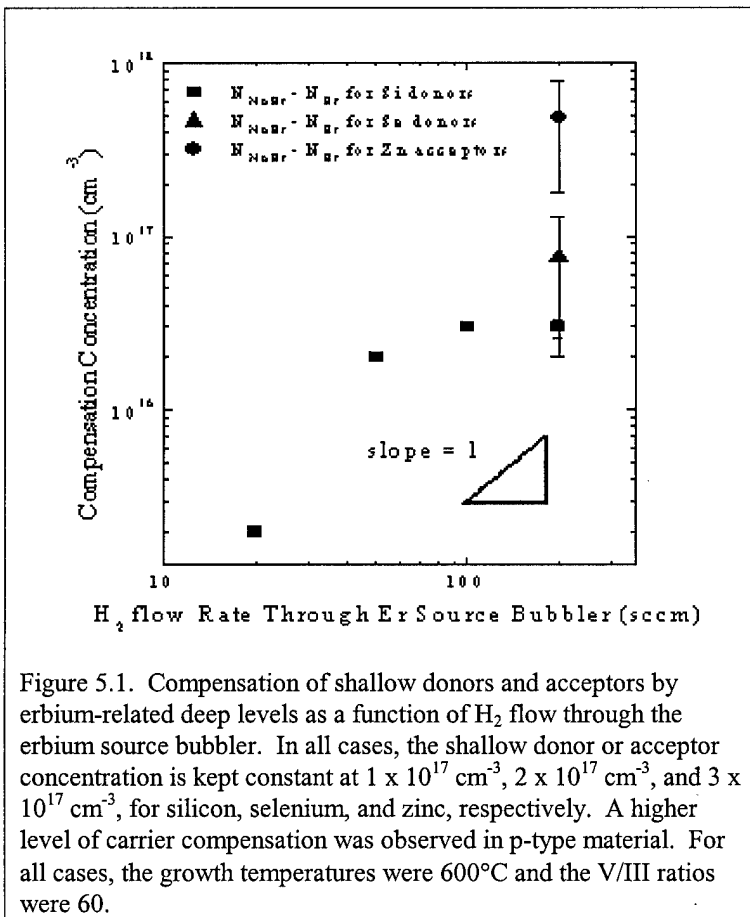


Figure 5.1. Compensation of shallow donors and acceptors by erbium-related deep levels as a function of H_2 flow through the erbium source bubbler. In all cases, the shallow donor or acceptor concentration is kept constant at $1 \times 10^{17} \text{ cm}^{-3}$, $2 \times 10^{17} \text{ cm}^{-3}$, and $3 \times 10^{17} \text{ cm}^{-3}$, for silicon, selenium, and zinc, respectively. A higher level of carrier compensation was observed in p-type material. For all cases, the growth temperatures were 600°C and the V/III ratios were 60.

background. An erbium precursor is presented in this study that is free from such 'unintentional' and undesired impurities. We have investigated the use of a new erbium precursor, tris(3,5-di-tert-butylpyrazolato)bis(4-tert-butylpyridine)erbium, abbreviated (t-Bu₂Pz)₃(4-t-BuPy)₂Er where Pz denotes a pyrazolato ligand and Py denotes a pyridine ligand, that contains no direct Er-C or Er-Si bonds. In this paper, a comprehensive study of the electrical and optical properties of GaAs films doped with erbium using this new precursor is presented. The effect of shallow impurities on the erbium-related luminescence is reported and several mechanisms for erbium-related luminescence quenching are discussed.

Results: The electrical compensation, $N_{\text{NoEr}} - N_{\text{Er}}$, where N is the carrier concentration, measured in GaAs:Er samples co-doped with silicon, selenium, or zinc is shown in Figure 5.1 as a function of the H_2 flow rate through the erbium source bubbler (related to the

5. Incorporation of optically active erbium into GaAs using the novel precursor tris(3,5-di-tert-butylpyrazolato)bis(4-tert-butylpyridine)erbium

Introduction: Semiconductors doped with rare-earth impurities are of scientific and technological interest. Rare-earth isoelectronic impurities incorporated into semiconductors would allow for the integration of optical and electronic components through the development of temperature invariant light sources in the near infrared (IR) spectral range for use in optical communication. Incorporation of erbium into silicon has been investigated for such optoelectronic applications. Compound semiconductors have also been investigated as rare-earth ion hosts with several advantages over these silicon based approaches that include a reduction of the thermal quenching of the luminescent lifetime and intensity.

Several erbium compounds have been previously investigated for use in MOVPE growth. Cyclopentadienyl (Cp)-based erbium sources have been most commonly used due to their ease of synthesis and their similarity to bis-cyclopentadienyl magnesium. Cp-based sources are often employed as volatile precursors for transition metal and lanthanide elements. Cp-based erbium sources have been shown to co-incorporate carbon into the GaAs films that could alter the microscopic environment of the erbium center. Sources based on amide ligand chemistries have also been investigated, but these source compounds can contain other potential impurities, such as silicon. Co-introduction of other unintentional impurities can result in the formation of undesirable erbium complexes and produce an n- or p-type

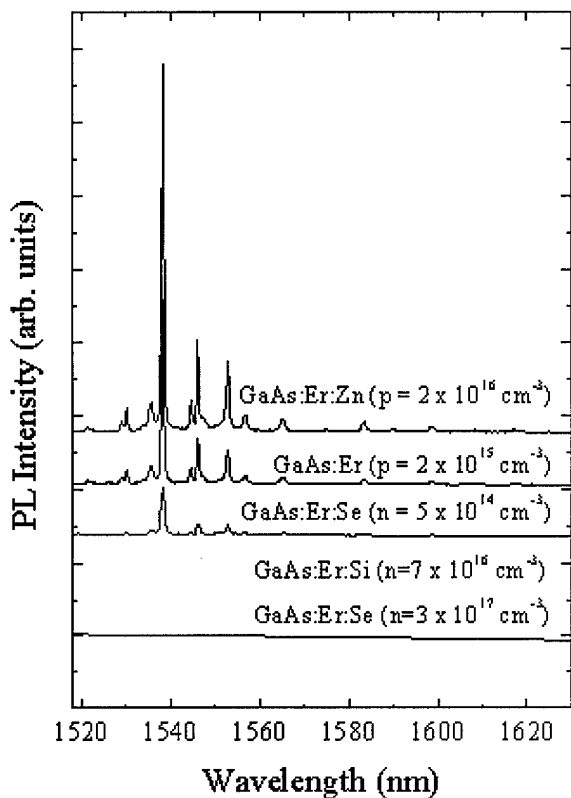


Figure 5.2. Photoluminescence spectra taken at 12 K for GaAs doped only with erbium and co-doped with zinc, selenium, and silicon. The PL intensity is decreased as the Fermi level approaches the conduction band. Samples grown at 600°C with a V/III of 60.

reduced, but not completely quenched. Co-doping with zinc, however, lead to a two-fold increase in the magnitude of the erbium-related luminescence as noted in Figure 5.2. DLTS measurements were taken over the 80-450 K temperature range with a representative DLTS spectrum for GaAs:Er:Si. Four deep levels, labeled as E1 through E4 were detected and parameters for these electron traps were determined from the Arrhenius plot.

The $(t\text{-Bu}_2\text{Pz})_3(4\text{-t-BuPy})_2\text{Er}$ source forms a specific erbium center in the GaAs film under our particular growth conditions. The erbium optical activity, attributed to the Er-2O center, was found to be very high when compared to centers found in GaAs films prepared with other erbium precursors. Cp-based erbium sources introduce several impurity centers leading to broad luminescence features, unless intentional oxygen is added to the reactor during growth. In the present study, the presence of unintentional oxygen during growth cannot be excluded. The unintentional oxygen in the present study may come from several sources. H_2O and tetrahydrofuran could be contaminants introduced during source synthesis. Both molecules, however, would react with pyrazolato ligands to produce a compound which is much less volatile than $(t\text{-Bu}_2\text{Pz})_3(4\text{-t-BuPy})_2\text{Er}$. The most likely sources of oxygen are therefore residual contaminants in the source gases or H_2O adsorbed on the inner reactor walls during sample loading. Metal-organic source materials, such as TMGa, can have trace amounts of metal alkoxides that lead to oxygen incorporation. The addition of shallow impurities to GaAs:Er has a strong influence on the 1.538 μm luminescence as seen in the spectra in Figure 5.2. Quenching of the erbium-related luminescence by shallow donors has been previously reported for material grown by MBE. In that case, the quenching was attributed to the formation of Er-Si moieties. Based on this present study, such complex formation is unlikely since both Se and Si co-doping results in the same quenching behavior. Si and Se reside on different sublattices, and may result in the formation of very different defect complexes. We believe that such Er-donor complexes do not, therefore, play a role in the quenching behavior seen in our MOVPE growth samples.

A likely mechanism for the quenching of the erbium-related luminescence is the presence of alternative pathways of energy transfer that compete with the pathway leading to the excited erbium ion. An existing model for the excitation of the erbium center involves the formation of a bound exciton on the Er^{3+} ion that recombines to create an excited Er^{3+} ion. A high electron and hole concentration would reduce the radiative lifetime for competing band-to-band recombination. Such rapid band-to-band recombination would decrease the erbium-related emission in both n- and p-type samples. The quenching of erbium-related emission in n-type material, but not p-type material, does not support this mechanism as the sole competing recombination pathway. Auger energy transfer involving the erbium-bound exciton or the excited Er^{3+} ion and a band-state electron could also lead to a decrease in erbium-related emission.

erbium mole fraction in the reactor). In silicon-doped GaAs:Er, the electrically active concentration appears to be slightly sub-linear with the compensation saturating at high H_2 (Er) flow rates. In zinc-doped GaAs:Er, a larger amount of compensation was observed for a similar erbium source flow rate. The compensation measured for n-type samples appears independent of donor species within our measurement uncertainty. The amount of compensation by erbium-related defects in p-type GaAs is almost one order of magnitude greater than that for n-type GaAs for the same gas phase erbium concentration. SIMS could not detect measurable amounts of erbium or oxygen, as monitored by ^{168}Er and ^{85}GaO ions, respectively, indicating that the concentration of these species were below the SIMS detection limits, which were $8 \times 10^{15} \text{ cm}^{-3}$ for ^{168}Er and $4 \times 10^{17} \text{ cm}^{-3}$ for ^{85}GaO . PL measurement on samples annealed in N_2 at 400°C and 500°C for 20 minutes did not exhibit any measurable change in the erbium-related emission, indicating the stability of the incorporated erbium. The erbium incorporation, based on EC-V compensation measurements, was reduced at increased growth temperatures, for the experimental conditions investigated. The degree of electrical compensation decreases with increased V/III ratio by approximately a factor of two over the range investigated. Higher V/III ratios can lead to a reduced unintentional carbon incorporation and a slight increase in the concentration of silicon donors from Si_2H_6 . These factors make determination of minor changes in compensation due to erbium difficult to separate from these temperature and V/III ratio effects.

Photoluminescence (PL) measurements of GaAs doped only with erbium yielded the spectrum shown in Figure 5.2. The features of this spectrum have been previously assigned to the Er-2O center. Co-doping with silicon or selenium leads to a quenching of the erbium-related luminescence, also shown in Figure 5.2. To further investigate the effect of shallow donors on the luminescence, GaAs:Se:Er having an electron concentration of only $n \sim 5 \times 10^{14} \text{ cm}^{-3}$ was grown. The intensity of the erbium-related luminescence is

An increased electron concentration would lead to an increase in non-radiative Auger recombination. The Auger recombination rate for n-type GaAs:Er is expected to be much higher than the rate for p-type GaAs:Er.

Conclusions: We have investigated a new source, tris(3,5-di-t-butylpyrazolato)bis(4-t-butylpyridine) erbium, for the incorporation of erbium into GaAs. Erbium is believed to incorporate in the form of an Er-2O center as is evidenced by the sharp luminescence spectrum characteristic of this specific defect. There is a dramatic effect of the sample carrier type on this erbium-related luminescence. The dependence of the erbium luminescence on the carrier type is proposed to be due to the formation of erbium complexes with native defects, which are present in higher concentrations in n-type material and enhanced Auger recombination in n-type GaAs. DLTS performed on a GaAs:Si:Er Schottky diode determined several deep levels in the upper half of the conduction band, which may be related to the luminescence quenching.

6. Photoluminescence and Free Carrier Interactions in Erbium-doped GaAs using a New Pyrazole and Pyridine-based Erbium Precursor

Introduction: We have investigated the characteristics of the $^4I_{13/2} \rightarrow ^4I_{15/2}$ Er^{3+} emission in GaAs:Er doped with pyrazole and pyridine-based Er sources. Although the concentration of Er incorporated into these samples was fairly low, the Er^{3+} emission was significantly stronger and sharper than in previous GaAs:Er samples doped with cyclopentadienyl-based Er sources. The efficient luminescence was associated with the Er-2O center, formed with unintentional oxygen impurities. Because of the encouraging emission characteristics in these samples despite the low Er concentration, our future work will attempt to preferentially form this Er-2O center in higher concentrations by using an intentional oxygen source. The source molecule could either be O_2 or $(C_2H_5)_2AlOC_2H_5$, which has been used to dope GaAs:O.

The Er^{3+} emission was greatly reduced in n-type samples, whereas the emission remained strong in p-type samples. One explanation is that the free hole concentration is very important to the Er^{3+} excitation efficiency, in that excess holes are needed to overcome thermalization of the Er-bound exciton through hole emission. A two-beam PL experiment was performed to examine these Auger quenching mechanisms. Both the decay lifetime and change in intensity induced by the modulated HeNe beam were measured as a function of the Ar beam excitation power. For the GaAs:Er sample ($p \sim 2 \times 10^{15} \text{ cm}^{-3}$ at room temperature), a sharp decrease in both the Er^{3+} lifetime and modulated intensity was observed even at very low Ar beam powers, suggesting that Auger quenching by excess free electrons was strong. The model developed indicates that a strong Auger quenching process is present, in which the bound exciton excites a free electron rather than the Er^{3+} ion. This quenching process might help explain the decrease in intensity observed in n-type samples. The alternate Auger quenching process, in which the excited Er^{3+} ion transfers its energy to a free electron, might be present, but is much less important. The Er^{3+} decay lifetime is 20-25% less in GaAs:Er,Se than in GaAs:Er or GaAs:Er,Zn, supporting that this process does play a minor role. At high temperatures, thermal quenching due to energy back-transfer was observed. At the lowest temperatures, the samples also showed a decrease in intensity. This effect was attributed to the freezing-out of carriers onto a relatively shallow trap which could be related to either Er or shallow impurities. We have observed several effects that show the importance of the interaction between Er centers and free carriers. In order to fully exploit the properties of these materials, an important goal will be a thorough understanding of these interactions.

Conclusions: The photoluminescence properties of GaAs:Er doped with a new pyrazole and pyridine-based Er source were investigated. These samples showed significantly stronger and sharper $1.54 \mu\text{m}$ Er^{3+} luminescence than in GaAs:Er samples doped with cyclopentadienyl-based Er sources. The efficient luminescence was associated with the Er-2O center, formed with unintentional oxygen impurities. The Er^{3+} emission was greatly reduced in n-type samples, whereas the emission remained strong in p-type samples. This trend suggests that either the free hole concentration is very important to the Er^{3+} excitation efficiency, and/or there is a strong Auger quenching mechanism which involves free electrons. Results from a two-beam experiment and a detailed model indicated the presence of strong Auger energy transfer from the Er-bound exciton to a free electron. Auger energy transfer from the excited Er^{3+} ion to a free electron was found to be much less important. The temperature dependence of the Er^{3+} emission was also examined. A decrease in intensity was observed at the lowest temperatures. This effect was attributed to the freezing-out of carriers onto a relatively shallow trap that could be related to either Er or shallow impurities.

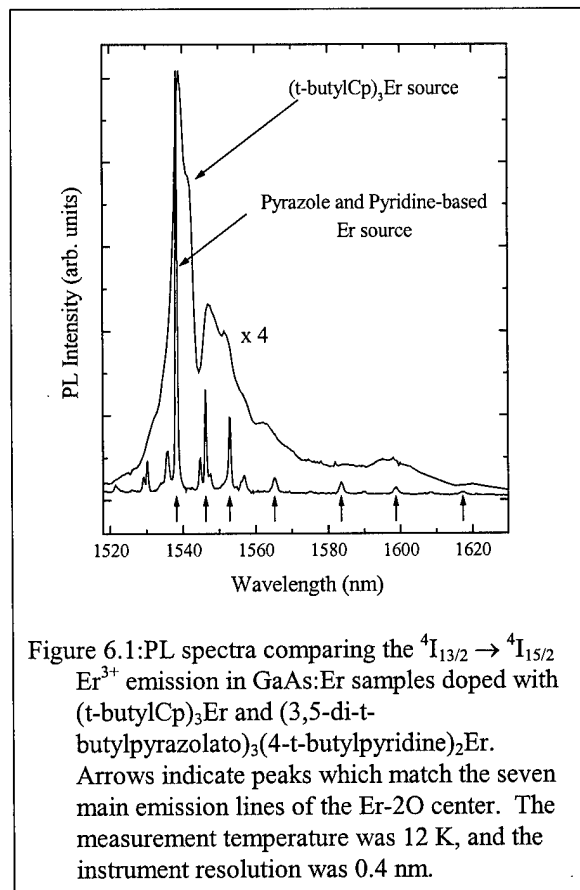


Figure 6.1: PL spectra comparing the $^4I_{13/2} \rightarrow ^4I_{15/2}$ Er^{3+} emission in GaAs:Er samples doped with $(t\text{-butylCp})_3\text{Er}$ and $(3,5\text{-di-t-butylpyrazolato})_3(4\text{-t-butylpyridine})_2\text{Er}$. Arrows indicate peaks which match the seven main emission lines of the Er-2O center. The measurement temperature was 12 K, and the instrument resolution was 0.4 nm.

7. INCORPORATION OF Er INTO GaN BY in-situ DOPING DURING HALIDE VAPOR PHASE EPITAXY

INTRODUCTION: The Er-doping into semiconductors has attracted a great deal of attention because of potential application to infrared optical fiber communications. The $\sim 1.54 \mu\text{m}$ emission due to intra-4f electron transition, $^4I_{13/2} \rightarrow ^4I_{15/2}$, of the Er^{3+} ions corresponds to a low loss transmission window of silica-based optical fibers. Because of the screening effect of the core levels in the partially filled 4f subshell by the filled $5s^2$ and $5p^6$ subshells, the Er^{3+} emission spectral features are nearly independent of the host material and temperature. The intensity of the $1.54 \mu\text{m}$ luminescence is strongly dependent on the temperature and the bandgap of the host material. The main synthesis technique for GaN:Er materials, to date, has been ion-implantation followed by a high temperature annealing step. After co-implanting Er and O ions into GaN or AlN and thermal annealing, sharp $\sim 1.54 \mu\text{m}$ Er^{3+} ion emission band is observed. We developed the successful *in-situ* doping of Er into GaN by HVPE using metallic Er source. The typical steady state doping concentration can be as high as $2 \times 10^{18} \text{cm}^{-3}$. Er surface segregation during growth has been observed in these samples. All *in-situ* Er-doped GaN samples present a sharp bandedge luminescence band. No yellow luminescence (YL) band is detected in any of the GaN:Er samples. The Er-doped GaN emits sharp $1.54 \mu\text{m}$ luminescence at both low and room temperatures. Higher Ga/Er source temperatures lead to stronger and sharper $1.54 \mu\text{m}$ Er ion luminescence.

RESULTS: All GaN:Er samples used in this study were grown on (0001) sapphire substrates in a horizontal atmospheric pressure HVPE system. NH_3 was used as the nitrogen source and its mole fraction was held constant at 0.11. GaCl and ErCl_3 , which were produced from the reaction between metallic Ga (7N) and Er (3N) in the Ga/Er boat and the introduced HCl, were used as Ga/Er source to grow GaN:Er films. The Ga/Er boat was set at a temperature either 850 or 880°C , while the substrate temperature remained at 1030°C . Formation of a miscible Ga-Er liquid requires an Er weight percentage less than 23% at 850°C and 27% at 880°C . In this study, the weight ratio of Er-to-Ga was set to 1:5. No other intentional dopants, besides Er, were used. All GaN:Er films are grown along the (0001) direction with a surface morphology that is dominated by large hexagonal features, which is typically observed for HVPE-grown GaN films. The surface is, however, much rougher for high Er-content GaN films than the unintentionally or C-doped GaN films, or films grown with H_2 addition into the growth ambient. Some cracks, many of them are very regular, can be seen in most samples due to thermal expansion mismatch during cooling. A few small pits appear along the cracks, particularly at the points of intersection of the cracks. The films exhibit n-type conductivity with the typical carrier concentration of $\sim 10^{19} \text{cm}^{-3}$ at room temperature. The samples grown at a Ga/Er source temperature of 850°C have a growth rate of $20 \mu\text{m/hr}$ and those grown with an 880°C metal source have a growth rate of $40 \mu\text{m/hr}$. A typical 880°C -metal source grown film showed a full-width-half-maximum (FWHM) of x-ray rocking curve of ~ 1098 arcsec while a typical 850°C -metal source grown sample gives ~ 677 arcsec.

Secondary ion mass spectroscopy (SIMS) was used to determine the doping concentration and depth profile in the HVPE-grown GaN films. The doping efficiency of the 880°C metal source growth (sample A metal source growth (sample B), which indicates that the doping efficiency is sensitive to the Ga/Er source temperature. The Er doping dynamics into GaN during HVPE is expected to be quite complicated. Initially, Er, in solution, reacts with HCl to produce ErCl_3 , which is the favored gas phase species. This present study can not discern the rate-limiting step in doping process. In all likelihood, oxide contamination on the surface of the Ga-Er source, expected given the high affinity of Er for oxygen, controls the Er transport rate from the source regime as well as potentially affecting the GaCl transport rate.

The PL spectra were obtained at both low and room temperatures. The 325 nm line from a HeCd laser was employed to stimulate the PL spectra. The excitation power density was 2.5 W/cm^2 . The PL signal was dispersed by a one-meter SPEX monochromator and collected by a cooled photomultiplier tube (PMT). Fig. 7.1 shows two typical low temperature ($T=11.5 \text{ K}$) PL spectra over the range of 1.78 - 3.55 eV . Fig. 7.1(a) and 7.1(b) are the PL spectra obtained from the sample A and sample B, respectively. Both spectra are normalized to their dominant luminescence bands. Strong bandedge (BE) luminescence band can be seen in both spectra. The BE peak energy of the sample A (B) is 3.47 eV (3.48 eV) and the FWHM is 32 meV (16 meV). Both spectrum (a) and (b) show wider BE band than that of unintentionally doped GaN grown under similar conditions at the same measurement temperature. The BE emission linetype of the sample A (a) has a greater asymmetry than that found in the sample B (b) spectrum. The long tail on the low-energy side of the BE peak in (a) is responsible for the broadening of the BE band as well as the red-shift of its peak position. This broadening of the BE band is attributed to a higher concentration of defects in the sample A than in the sample B in agreement with the above mentioned high-resolution x-ray diffraction data. No YL signal is detectable in all GaN:Er samples used in this study.

The $\sim 1.54 \mu\text{m}$ luminescence can be detected from GaN:Er films at both room and low temperature. Fig. 7.2 presents low-temperature PL spectra around $1.54 \mu\text{m}$ of sample A and B. Both samples A and B emit strong Er-ion based luminescence with the peak $\sim 1.54 \mu\text{m}$. Despite the poorer crystal quality in the sample A, the $1.54 \mu\text{m}$ luminescence intensity in this sample is 20 times higher than that of the sample B. The $1.54 \mu\text{m}$ luminescence intensity is primarily dependent on the Er^{3+} concentration in the GaN film.

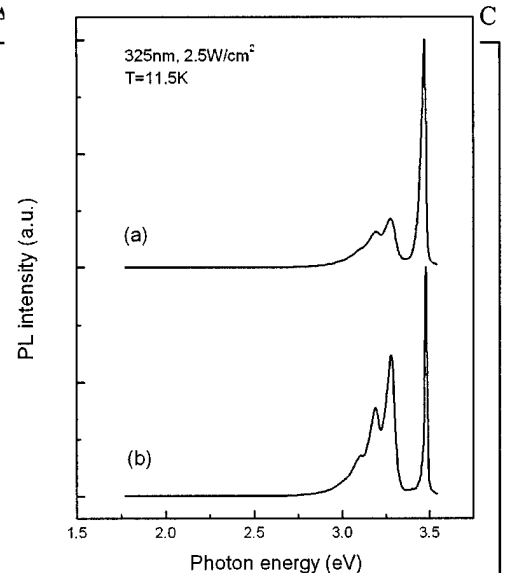


Fig. 7.1 Low-temperature (11.5K) PL spectra of the GaN:Er sample A (a) and B (b). No yellow luminescence can be detected. The broadened bandedge luminescence band in (a) over (b) indicates a higher defect density in the sample A than in the sample B.

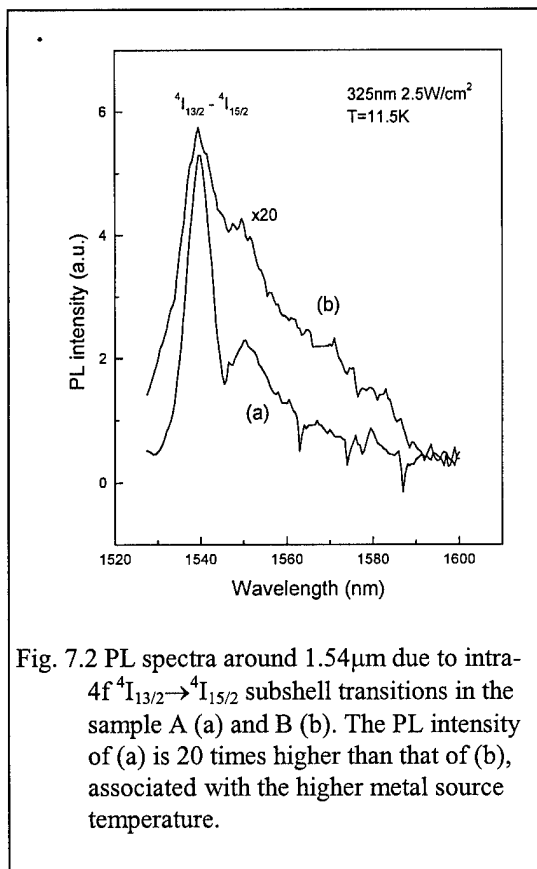


Fig. 7.2 PL spectra around 1.54 μm due to intra-4f $^4I_{13/2} \rightarrow ^4I_{15/2}$ subshell transitions in the sample A (a) and B (b). The PL intensity of (a) is 20 times higher than that of (b), associated with the higher metal source temperature.

At a 325 nm excitation wavelength, the estimated depth sampled by the PL is ~100 nm. The difference of Er concentration near the surface between the sample A and B, and thus the difference of the 1.54 μm Er^{3+} ions emission intensity between two samples, is not as large as that in the bulk of the films. The strength of the 1.54 μm spectral feature is also affected by the presence of additional impurities that serve as electronegative ligands accompanying with the Er atom. Er atoms surrounded by a strongly electronegative ligand field can lead to a high internal quantum efficiency of the Er^{3+} intra-4f transition, $^4I_{13/2} \rightarrow ^4I_{15/2}$. O, C, N, F, and S, are some of these ligands producing efficient 1.54 μm luminescence. Since only erbium was intentionally doped into the GaN:Er samples, the limited presence of these ligands could be limiting the observed 1.54 μm Er^{3+} ions luminescence intensity.

Unlike most Er-implanted GaN samples, there is no additional luminescence peak observed over the wavelength range from 1050 nm to 1400 nm, which is believed to be due to implantation-related damage. The additional luminescence peak due to the intra-4f transition, $^4I_{11/2} \rightarrow ^4I_{15/2}$, is found around 1000 nm at both low and room temperature from the sample A.

CONCLUSIONS: The incorporation of Er into GaN by *in-situ* doping during halide vapor phase epitaxy has been investigated. The NH_3 , HCl, metallic Ga and Er were used as source materials, while N_2 was employed as a carrier gas. The GaN:Er films were obtained at different Ga/Er source temperatures. The SIMS analysis shows that the steady state Er doping concentration can be as high as $2 \times 10^{18} \text{ cm}^{-3}$. All *in-situ* Er-doped samples luminescence at 1.54 μm due to the $^4I_{13/2} \rightarrow ^4I_{15/2}$ transition of Er^{3+} at both low (11K) and room temperature. The higher the Ga/Er boat temperature, the stronger the 1.54 μm luminescence, implying a higher incorporation rate of Er into the GaN. The $^4I_{11/2} \rightarrow ^4I_{15/2}$ transition luminescence, centered around 980 nm, can also be detected at both low

and room temperature. The broad-spectrum PL measurements exhibited sharp bandedge luminescence without the presence of the yellow luminescence band.

Listing of Publications Associated with this Grant:

1. "Ultrafast Photodetector Materials Based on Oxygen-Doped MOVPE GaAs", M.Y. Frankel, J.W. Huang, and T.F. Kuech, Appl. Phys. Lett. 66 (1995) 634-636.
2. "Controlled Oxygen Incorporation in Indium Gallium Arsenide and Indium Phosphide Grown by Metalorganic Vapor Phase Epitaxy", J.W. Huang, J.M. Ryan, K.L. Bray and T.F. Kuech, J. Electronic Materials 24(11) (1995) 1539-1546.
3. "Oxygen Levels in Metalorganic Vapor Phase Epitaxy Indium Gallium Arsenide", J.-W. Huang, T.F. Kuech, and T.J. Anderson, Appl. Phys. Lett. 67 (1995) 1116-1118.
4. "Intentional Defect Incorporation in MOVPE Indium Gallium Arsenide by Oxygen Doping", J.W. Huang and T.F. Kuech, Mat. Res. Soc. Symp. Proc. 378 (1995) 165-170.
5. "The Uniformity of Surface Passivation After $(NH_4)_2S$ Treatment Studied by Near-Field Scanning Optical Microscopy", Jutong Liu and T.F. Kuech, Mat. Res. Soc. Symp. Proc. 405 (1996) 415-420 and Mat. Res. Soc. Symp. Proc. 406 (1996) 523-528.
6. **Book Chapter:** "Chemical Vapor Deposition For Epitaxial Growth", T.F. Kuech, Electronics Materials Chemistry, Ed. B. Pogue, Marcel Dekker, Inc., Boston, 1996.
7. "Influence of Oxygen on Surface Morphology of Metalorganic Vapor Phase Epitaxy Grown GaAs (001)", S. Nayak, J.W. Huang, J. M. Redwing, D.E. Savage, M.G. Lagally, and T.F. Kuech, Appl. Phys. Lett. 68 (1996) 1270-1272.
8. "Interface Structures of InGaAs/InGaAsP/InGaP Quantum Well Laser Diodes Grown by Metal Organic Chemical Vapor Deposition on GaAs Substrates", A. Bhattacharya, L.J. Mawst, S. Nayak, J. Li, and T.F. Kuech, Appl. Phys. Lett., 68 (1996) 2240-2242.
9. "Electrical Characterization of Mg-doped GaN grown by Metalorganic Vapor Phase Epitaxy", J.W. Huang, T.F. Kuech, H. Lu, and I. Bhat, Appl. Phys. Lett. 68 (1996) 2392-2394.
10. "A Near-Field Scanning Optical Microscopy Study of the Uniformity of GaAs Surface Passivation", J. Liu and T.F. Kuech, Appl. Phys. Lett. 69 (1996) 662-664.
11. "A Near-Field Scanning Optical Microscopy Study of the Photoluminescence From GaN Films", Jutong Liu, N.R. Perkins, M.N. Horton, J.M. Redwing, M.A. Tischler, and T.F. Kuech, Appl. Phys. Lett. 69 (1996) 3519-3521.
12. "Chemical and Physical Effects in Oxygen Incorporation During Metal-organic Vapor Phase Epitaxial Growth of GaAs", T.F. Kuech, S. Nayak, J.-W. Huang, and J. Li, J. Crystal Growth 163 (1996) 171-179.

13. "Compensation of shallow impurities in oxygen-doped metal organic vapor phase epitaxy grown GaAs", J. W. Huang, K.L. Bray and T. F. Kuech, *J. Appl. Phys.* 80 (1996) 6819-6826.
14. "Oxygen-Related Defects in High Purity MOVPE AlGaAs", J.M. Ryan, J.W. Huang, T.F. Kuech and K.L. Bray, *Mat. Res. Soc. Symp. Proc.* 421 (1996) 27-32.
15. "Excitation Properties of Er-Doped GaP From Photoluminescence and High Pressure Studies", T.D. Culp, X.Z. Wang, T.F. Kuech, B. W. Wessels, and K.L. Bray, *Mater. Res. Soc. Symp. Proc.* 422 (1996) 279-284.
16. "Surface Morphology of Carbon-Doped GaAs Grown by MOVPE", Jiang Li and T.F. Kuech, *J. Crystal Growth* 170 (1997) 292-296.
17. "GaN Films Studied by Near-Field Scanning Optical Microscopy, Atomic Force Microscopy and High Resolution X-ray Diffraction", Jutong Liu, Dan Zhi, J.M. Redwing, M.A. Tischler, and T.F. Kuech, *J. Crystal Growth* 170 (1997) 357-361.
18. "Ultrafast Carrier Trapping in Oxygen-doped Metal-organic Vapor Phase Epitaxy GaAs", J. U. Kang, M.Y. Frankel, J.-W. Huang and T.F. Kuech, *Appl. Phys. Lett.* 70 (1997) 1560-1562.
19. "Photoluminescence Studies of Erbium-Doped GaAs under Hydrostatic Pressure", T.D. Culp, U. Hömmerich, J.M. Redwing, T.F. Kuech, and K.L. Bray, *J. Appl. Phys.* 82 (1) July 1977, 368-374.
20. "Oxygen-Related Defects in Low Phosphorous Content GaAs_{1-y}P_y Grown by MOVPE", J.G. Cederberg, K.L. Bray and T.F. Kuech, *J. Appl. Phys.* 82 (1997) 2263-2269.
21. "Evolution of Surface Structure during Carbon Doping in the Metal Organic Vapor Phase Epitaxial Growth of GaAs", J. Li and T.F. Kuech, *J. Crystal Growth* 181 (1997) 171-180.
22. "Spatial Resolution of Localized Photoluminescence by Near-Field Scanning Optical Microscopy", S.A. Safvi, J. Liu and T.F. Kuech, *J. Appl. Phys.*, 82 (1997) 5352-5359.
23. "Photoluminescence of Erbium-implanted GaN and in situ-doped GaN:Er", D.M. Hansen, R. Zhang, N.R. Perkins, S. Safvi, L. Zhang, K.L. Bray and T.F. Kuech, *Appl. Phys. Lett.* 72 (1998) 1244-1246.
24. "Photoluminescence of Carbon in-situ Doped GaN Grown by Halide Vapor Phase Epitaxy", R. Zhang and T.F. Kuech, *Appl. Phys. Lett.* 72 (1997) 1611-1613.
25. "Photoluminescence and Free Carrier Interactions in Erbium-doped GaAs using a New Pyrazole and Pyridine-based Erbium Precursor", T.D. Culp, J.G. Cederberg, B. Bieg, T.F. Kuech, K.L. Bray, D. Pfeiffer and C.H. Winter, *J. Appl. Phys* 83(9) (1998) 4918-4927.
26. "Oxygen-related Defects in In_{0.5}(Al_xGa_{1-x})_{0.5}P Grown by MOVPE," J.G. Cederberg, B. Bieg, J.W. Huang, S.A. Stockman, M.J. Peanasky, and T.F. Kuech, *Mat. Res. Soc. Symp. Proc. Vol. 484* (1998) 611-615.
27. "Influence of C, N and O Ion-Implantation on Yellow Luminescence", R. Zhang, L. Zhang, N. Perkins, and T.F. Kuech, *Mat. Res. Soc. Symp. Proc.* 512 (1998) 321-326.
28. "Incorporation of Er into GaN by in-situ Doping During Halide Vapor Phase Epitaxy", R. Zhang and T.F. Kuech, *Mat. Res. Soc. Symp. Proc.* 512 (1998) 327-331.
29. "Intrinsic and Oxygen-Related Defects In In_{0.5}(Al_xGa_{1-x})_{0.5}P Grown By MOVPE", J. G. Cederberg, B. Bieg, J.- W. Huang, S. A. Stockman, M. J. Peanasky, and T. F. Kuech, *J. Crystal Growth* 195 (1998) 63-68.
30. "Erbium-doped GaAs Grown Using the Novel Precursor tris(3,5-di-tert-butylpyrazolato)bis(4-tert-butylpyridine)erbium", J. G. Cederberg, T. D. Culp, B. Bieg, D. Pfeiffer, C. H. Winter, K. L. Bray, and T. F. Kuech, *J. Crystal Growth* 195 (1998) 105-111.
31. "Effect Of Interface Roughness On Performance Of AlGaAs/InGaAs/GaAs Resonant Tunneling Diodes", Jiang Li, A. Mirabedini, L. J. Mawst, D. E. Savage, R. J. Matyi, and T. F. Kuech, *J. Crystal Growth* 195 (1998) 617-623.
32. "Impurity Incorporation and the Surface Morphology of MOVPE Grown GaAs", Jiang Li and T.F. Kuech, *J. Electron. Mater.* 28(2), 124-133 (1999).

Presentations with Peer-reviewed, Published Abstracts

- 1) "Controlled Oxygen Incorporation in In_xGa_{1-x}As and InP Grown by Metal-Organic Vapor Phase Epitaxy", J.W. Huang, and T.F. Kuech, 7th Biennial Workshop on Organometallic Vapor Phase Epitaxy, Ft. Myers, FLA, April 2-6, 1995.
- 2) "Impurity Induced Step Bunching and Faceting During MOVPE Growth of GaAs", T.F. Kuech, and S. Nayak, 7th Biennial Workshop on Organometallic Vapor Phase Epitaxy, Ft. Myers, FLA, April 2-6, 1995.
- 3) "Quantitative Study of MOCVD Grown InGaAs/InGaAs/InGaP Quantum Wells on GaAs Substrates", A. Bhattacharya, L.J. Mawst, Jiang Li, S. Nayak, and T.F. Kuech, 1995 Electronic Materials Conference, Charlottesville, VI, June 21-23, 1995.
- 4) "Oxygen-Based Deep Levels Incorporated in Metalorganic Vapor Phase Epitaxy InP", J.W. Huang and T.F. Kuech, 1995 Electronic Materials Conference, Charlottesville, VI, June 21-23, 1995.
- 5) "Similarities in the Photoluminescence Properties of Oxygen-Doped GaAs and Nominally Undoped AlGaAs", Michael Ryan, Jen-wu Huang, T.F. Kuech, and K.L. Bray, 1995 Electronic Materials Conference, Charlottesville, VI, June 21-23, 1995.
- 6) "Photoluminescence of Erbium-Doped III-V Semiconductors Under High Pressure", T. D. Culp, U. Hommerich, J.M. Redwing, T.F. Kuech, and K.L. Bray, 1995 Electronic Materials Conference, Charlottesville, VI, June 21-23, 1995.
- 7) "HVPE Growth of GaN Films on Sapphire and Si Substrates", N.R. Perkins, M.N. Horton, and T.F. Kuech, American Institute of Chemical Engineering Meeting, Miami, FLA, April 8-12, 1995.

- 8) "The Uniformity of Surface Passivation After $(\text{NH}_4)_2\text{S}$ Treatment Studied by Near-Field Scanning Optical Microscopy", Jutong Liu and T.F. Kuech, Materials Research Society Meeting, Boston, MA, Nov. 27-12/1, 1995.
- 9) "Halide Vapor Phase Growth of GaN Films on Sapphire and Si Substrates", N.R. Perkins, M.N. Horton, and T.F. Kuech, Materials Research Society Meeting, Boston, MA, Nov. 27-12/1, 1995.
- 10) "Excitation Properties of Erbium-Doped Gallium Arsenide from Photoluminescence and High Pressure Studies", T.D. Culp, T.F. Kuech, and K.L. Bray, American Physical Society Meeting, St. Louis, MO, March, 1996.
- 11) "Photoluminescent and High Pressure Study of MOVPE GaAs Co-doped with Oxygen and Shallow Impurities", J.M. Ryan, J.W. Huang, T.F. Kuech, and K.L. Bray, American Physical Society Meeting, St. Louis, MO, March, 1996.
- 12) "A Study of Electrical Properties of Mg-Doped GaN Grown by Metalorganic Vapor Phase Epitaxy", J.W. Huang, T.F. Kuech, H. Lu, I. Bhat, American Physical Society Meeting, St. Louis, MO, March, 1996.
- 13) "Photoluminescence Studies of Er-Doped Gallium Arsenide Under High Pressure", T.D. Culp, U. Hommerich, J.M. Redwing, T.F. Kuech and K.L. Bray, Materials Research Society Meeting, San Francisco, CA, April 8-12, 1996.
- 14) "High Temperature Gas phase Reactions of Trimethyl Gallium with NH_3 and Trimethyl Amine", A. Thon, S.A. Safvi and T.F. Kuech, Materials Research Society Meeting, San Francisco, CA, April 8-12, 1996.
- 15) "Electrical Characterization of Magnesium-Doped Gallium Nitride Grown by Metalorganic Vapor Phase Epitaxy, J.W. Huang and T.F. Kuech, Hongqiang Lu and Ishwara Bhat, Materials Research Society Meeting, San Francisco, CA, April 8-12, 1996.
- 16) "Excitation Properties of Er-Doped GaP and GaAs From Photoluminescence and High Pressure Studies", T.D. Culp, U. Hömmerich, J.M. Redwing, X.Z. Wang, B. W. Wessels, T.F. Kuech and K.L. Bray, Materials Research Society Meeting, San Francisco, CA, April 8-12, 1996.
- 17) "Oxygen-Related Defects in High Purity MOVPE AlGaAs", J.M. Ryan, J.W. Huang, T.F. Kuech and K.L. Bray, Materials Research Society Meeting, San Francisco, CA, April 8-12, 1996.
- 18) "High Spatial Resolution Photoluminescence Measurements of GaN by Near-Field Scanning Optical Microscopy", Jutong Liu, N.R. Perkins, M.N. Horton, J.M. Redwing, M.A. Tischler, and T.F. Kuech, Materials Research Society Meeting, San Francisco, CA, April 8-12, 1996.
- 19) "GaN Photoluminescence Measurements by Near-field Scanning Optical Microscopy with High Spatial Resolution", T.F. Kuech, N. Perkins, M. Horton, J. Liu, International Conference on Metalorganic Vapor Phase Epitaxy VIII, Cardiff, Wales, June 9-13, 1996.
- 20) "Surface and Interface Morphology of carbon-doped GaAs Grown by MOVPE", Jiang Li and T.F. Kuech, International Conference on Metalorganic Vapor Phase Epitaxy VIII, Cardiff, Wales, June 9-13, 1996.
- 21) "Oxygen Related Defects in Low Phosphorus Content $\text{GaAs}_{1-y}\text{P}_y$ Ternary Alloys Grown by MOVPE", J.G. Cederberg and T.F. Kuech, Electronic Materials Conference, Santa Barbara, CA, June 26-28, 1996.
- 22) "Resolution Limits of Localized Photoluminescence Measurements Using Near-field Scanning Optical Microscopy", Jutong Liu, S.A. Safvi, and T.F. Kuech, Electronic Materials Conference, Santa Barbara, CA, June 26-28, 1996.
- 23) "Impurity Incorporation and the Surface Morphology of MOVPE-Grown GaAs", Jiang Li and T.F. Kuech, Biennial Workshop on Metal Organic Vapor Phase Epitaxy, Dana Point, CA, April 13-17, 1997.
- 24) "Oxygen related defects in $\text{Al}_{0.46}\text{In}_{0.54}\text{P}$ Alloys grown by MOVPE", J.G. Cederberg, S.A. Stockman, M.J. Peanasky and T.F. Kuech, Electronic Materials Conference, Fort Collins, CO, June 24-26, 1997.
- 25) "Photoluminescence Studies of Erbium-doped GaAs using a New Pyrazole and Pyridine-Based Erbium Source", T.D. Culp, J.G. Cederberg, D. Pfeiffer, C.H. Winter, K.L. Bray, and T.F. Kuech, Electronic Materials Conference, Fort Collins, CO, June 24-26, 1997.
- 26) "Carbon and Hydrogen Induced Yellow Luminescence in Gallium Nitride Grown by Halide Vapor Phase Epitaxy", R. Zhang and T.F. Kuech, Materials Research Society Meeting, Boston, MA, Dec. 1-5, 1997.
- 27) "Oxygen Related Defects in $\text{In}_{0.5}(\text{Al}_x\text{Ga}_{1-x})_{0.5}\text{P}$ Quaternary Alloys Grown by MOVPE", J.G. Cederberg, B. Bieg, J-W Huang, M.J. Peanasky, S.A. Stockman and T.F. Kuech, Materials Research Society Meeting, Boston, MA, Dec. 1-5, 1997.
- 28) 'Influence of C, N and O ion-implantation on yellow luminescence', R. Zhang, L. Zhang, N. Perkins and T.F. Kuech, MRS Spring 1998 Meeting, San Francisco, CA, April 13-17, 1998.
- 29) 'Incorporation of Er into GaN by in-situ doping in Halide Vapor Phase Epitaxy', Rong Zhang and T.F. Kuech, MRS Spring 1998 Meeting, San Francisco, CA, April 13-17, 1998.
- 30) 'Oxygen Related Defects In $\text{In}_{0.5}(\text{Al}_x\text{Ga}_{1-x})_{0.5}\text{P}$ Quaternary Alloys Grown By MOVPE', J. G. Cederberg, B. Bieg, J.- W. Huang, M. J. Peanasky, S. A. Stockman, T. F. Kuech, The Ninth International Conference on Metal Organic Vapor Phase Epitaxy (ICMOVPE IX), LaJolla, CA, May 31- June 4, 1998.
- 31) 'DLTS Studies Of Deep Levels In Er Doped GaAs And $\text{Al}_x\text{Ga}_{1-x}\text{As}$ Grown By MOVPE', J. G. Cederberg, T. D. Culp, B. Bieg, D. Pfeiffer, C. H. Winter, K. L. Bray, and T. F. Kuech, The Ninth International Conference on Metal Organic Vapor Phase Epitaxy (ICMOVPE IX), LaJolla, CA, May 31- June 4, 1998.

Personnel Supported:**Graduate Students Receiving Support**

All listed have been partial support. Their research activities are indicated.

Name	Current Position	Activity
Jen-wu Huang	Ph.D., Ch.E., Hewlett-Packard, Corp.	Defect Characterization
Jiang Li	Ph.D., Ch.E., now at AMD Corp.	Impurity effects at surfaces
Eric Rehder	Current Materials Science Program Ph.D. Student	Surface and structural characterization
Jeff Cederberg	Current ChE Ph.D. Student	Growth of Oxygen Doped Alloys
Fransiska Dwikusuma	Current ChE Ph.D. Student	HVPE Growth of GaN and contactless Electroreflectance
Ling Zhang	Current ChE Ph.D. Student	MOVPE Growth of Semiconductors
Darren Hansen	Current ChE Ph.D. Student	FTIR measurements of defects
Brian Hawkins	Current ChE Ph.D. Student	DLTS measurements

Postdoctoral Fellows Receiving Support

All listed have been partial support. Their research activities are indicated.

Name	Current Position	Activity
Shulin Gu	Visiting Professor from Nanjing University	Materials growth and spectroscopy

Other Personnel Impacted By and Participating in Research Supported by the Grant but not Receiving Support

Name	Position	Activity
Bordan Bieg	Visiting Scientist, return to Warsaw University	Defect spectroscopy
Peter Moran	Research Scientist, UW-Madison	Materials Synthesis